MOLECULAR AND CELLULAR BIOLOGY, June 2008, p. 4004–4017 Vol. 28, No. 12
0270-7306/08/$08.00+0 doi:10.1128/MCB.00157-08

Identification of Proteins Associating with Glycosylphosphatidylinositol-Anchored T-Cadherin on the Surface of Vascular Endothelial Cells: Role for Grp78/BiP in T-Cadherin-Dependent Cell Survival▽†

Maria Philippova,[1]* Danila Ivanov,[1] Manjunath B. Joshi,[1] Emmanouil Kyriakakis,[1] Katharina Rupp,[1] Taras Afonyushkin,[2] Valery Bochkov,[2] Paul Erne,[3] and Therese J. Resink[1]

Department of Research, Cardiovascular Laboratories, Basel University Hospital, Hebelstrasse 20, CH 4031 Basel, Switzerland[1]; Department of Vascular Biology and Thrombosis Research, Medical University of Vienna, Schwarzspanierstrasse 17, 1090 Vienna, Austria[2]; and Division of Cardiology, Luzern Kantonsspital, CH 6000 Luzern, Switzerland[3]

Received 30 January 2008/Returned for modification 9 March 2008/Accepted 2 April 2008

There is scant knowledge regarding how cell surface lipid-anchored T-cadherin (T-cad) transmits signals through the plasma membrane to its intracellular targets. This study aimed to identify membrane proteins colocalizing with atypical glycosylphosphatidylinositol (GPI)-anchored T-cad on the surface of endothelial cells and to evaluate their role as signaling adaptors for T-cad. Application of coimmunoprecipitation from endothelial cells expressing c-*myc*-tagged T-cad and high-performance liquid chromatography revealed putative association of T-cad with the following proteins: glucose-related protein GRP78, GABA-A receptor α1 subunit, integrin β_3, and two hypothetical proteins, LOC124245 and FLJ32070. Association of Grp78 and integrin β_3 with T-cad on the cell surface was confirmed by surface biotinylation and reciprocal immunoprecipitation and by confocal microscopy. Use of anti-Grp78 blocking antibodies, Grp78 small interfering RNA, and coexpression of constitutively active Akt demonstrated an essential role for surface Grp78 in T-cad-dependent survival signal transduction via Akt in endothelial cells. The findings herein are relevant in the context of both the identification of transmembrane signaling partners for GPI-anchored T-cad as well as the demonstration of a novel mechanism whereby Grp78 can influence endothelial cell survival as a cell surface signaling receptor rather than an intracellular chaperone.

T-cadherin (T-cad, or H-cadherin or cadherin-13) is an atypical member of the cadherin superfamily of adhesion molecules. The "classical" cadherins are transmembrane receptors that mediate homophilic Ca^{2+}-dependent adhesion between the cells of solid tissues (2). The extracellular domain organization of T-cad is similar to that of classical cadherins, but it lacks transmembrane and cytosolic domains and is attached to the plasma membrane by a glycosylphosphatidylinositol (GPI) anchor (57). T-cad was shown to mediate weak homophilic cell aggregation in suspensions of transfected cells (45, 57). However, there is a large amount of data suggesting that, in contrast to classical cadherins, atypical T-cad does not primarily function in the maintenance of intercellular adhesion; T-cad is not concentrated at sites of cell-cell contacts, is expressed on the luminal but not the baso-lateral surface of polarized transfected cells, and locates in lipid raft domains of the plasma membrane (29, 42, 43). In the embryonic nervous system T-cad functions as a negative guidance cue regulating motor axon outgrowth and innervation of skeletal muscle (15). Many studies in the cancer field have demonstrated a relationship between T-cad expression levels in tumor cells and tumor progression, although its influence on cell behavior varies in different cancer types, either inhibiting invasion and growth or correlating with a high proliferative and invasive potential (46, 52).

In the cardiovascular system T-cad is highly expressed on endothelial cells (ECs), smooth muscle cells, and cardiomyocytes. Its expression level is increased in atherosclerotic lesions from the human aorta (22), in experimental restenosis during neointima formation after balloon catheterization of rat carotid artery (30), and in ECs from tumor vasculature (59). Together, these data suggest that upregulation or/and ligation of T-cad molecules on vascular cells might importantly contribute to progression of vascular pathologies associated with vascular tissue remodelling and stress, such as atherosclerosis, restenosis, and neovascularization of atherosclerotic lesions or tumors. This hypothesis is supported by studies showing that overexpression and/or homophilic ligation of T-cad in ECs stimulates proliferation, migration, and survival under conditions of oxidative stress and promotes angiogenesis in vitro and in vivo (21, 23, 26, 40).

Signaling mechanisms underlying T-cad effects on cell growth and motility are poorly studied. We have identified some target signaling pathways activated in cultured vascular ECs by surface T-cad. Changes in cell phenotype during T-cad ligation-induced migration depend on activation of RhoA and Rac GTPases (41). Overexpression and/or ligation of T-cad induces increases in Akt and GSKβ3 phosphorylation levels and activation of β-catenin, and all these effects are blocked by phosphatidylinositol 3-kinase (PI3-kinase) inhibitors (26).

There is scant knowledge regarding how cell surface lipid-anchored T-cad transmits signals through the plasma membrane to its intracellular targets. The absence of transmembrane and

* Corresponding author. Mailing address: Cardiovascular Laboratories, Basel University Hospital, Hebelstrasse 20, CH 4031 Basel, Switzerland. Phone: 41 61 265 2967. Fax: 41 61 265 2350. E-mail: maria.filippova@unibas.ch.

† Supplemental material for this article may be found at http://mcb.asm.org/.

▽ Published ahead of print on 14 April 2008.

cytoplasmic domains implies the existence of transmembrane "adaptors" that interact with T-cad on the outer surface of the plasma membrane. Data in the current literature do not allow prediction of membrane associations of T-cad, which from the structural point of view shares homology with two distinct protein groups, namely, cadherins and GPI-anchored proteins. Absence of the cytoplasmic domain excludes any possibility of direct interactions between T-cad and molecular mechanisms utilized by classical cadherins, such as catenins. Recently we have demonstrated that T-cad overexpression results in stimulation of β-catenin signaling in ECs (25). However, this effect is the consequence of Akt/GSK3β pathway activation rather than the result of a direct physical interaction with β-catenin. A requirement for integrin-linked kinase (ILK) upstream of Akt/GSKβ3/β-catenin modulation by T-cad has recently been shown (25). However, ILK is located intracellularly and thus cannot function as a primary molecular adaptor for surface T-cad.

The presence of a lipid GPI anchor on the C terminus of the T-cad molecule suggests that T-cad may utilize some of the signaling mechanisms that depend on its localization within lipid rafts, cholesterol- and sphingolipid-rich domains of the plasma membrane that act as signal transduction platforms compartmentalizing, clustering, and facilitating interactions between various lipid-anchored signaling molecules (49). However, the group of GPI proteins is highly heterogeneous both structurally and functionally and includes membrane-associated enzymes, adhesion receptors, differentiation markers, protozoan coat components, and other miscellaneous glycoproteins. Likewise, downstream raft-associated signaling is also diverse, including small GTPases, Src kinases, lipid second messengers, and many others (20). Moreover, molecular interactions within lipid rafts have been shown to be determined by many factors, such as the presence of receptor ligands, their precise membrane localization (the leading edge versus overall surface distribution), and lipid composition (ganglioside GM1-enriched versus GM3-enriched lipid rafts), among others (7).

This study aimed to identify membrane proteins colocalizing with atypical GPI-anchored T-cad on the surface of cultured ECs and to evaluate the role of identified molecules as adaptors transmitting signals from cell surface T-cad to its intracellular targets. We have identified several candidate proteins with potential functions as membrane adaptors for T-cad, namely, glucose-related protein Grp78/BiP, GABA-A receptor α1 subunit, integrin β_3, and two hypothetical proteins, LOC124245 and FLJ32070. We demonstrate that the interaction between T-cad and surface Grp78 is necessary for T-cad-dependent activation of prosurvival signaling in ECs.

MATERIALS AND METHODS

Cell culture. Human endothelial cells from umbilical vein (HUVEC) were purchased from PromoCell GmbH (Heidelberg, Germany) and cultured on plates precoated with 0.1% gelatin in EC growth medium containing EC growth supplement (PromoCell). HUVEC between passages 2 and 6 were used in the experiments described herein. Human microvascular EC line HMEC-1 (1) was cultured in the same medium supplemented with 10% fetal calf serum. HEK 293T and HeLa cells were cultured in Dulbecco's modified Eagle's medium supplemented with penicillin-streptomycin and 10% fetal calf serum (Gibco, Basel, Switzerland).

Antibodies. The following primary antibodies were used: polyclonal antibody against the first extracellular domain of human recombinant T-cad (22); goat polyclonal anti-T-cad immunoglobulin G (IgG; R&D Systems Europe Ltd., Abingdon, United Kingdom), mouse anti-c-*myc*, anti-integrin β_3, anti-VE-cadherin, and anti-Grp78 IgG (BD Biosciences, Basel, Switzerland); rabbit and goat anti-Grp78 IgG (Santa Cruz Biotechnology, Heidelberg, Germany); mouse anti-integrin $\alpha_V\beta_3$ monoclonal antibody 1976Z (Chemicon, Rueschlikon, Switzerland); anti-glyceraldehyde-3-phosphate dehydrogenase (anti-GAPDH) IgG (Abcam, Cambridge, United Kingdom); anti-Akt, anti-phospho-(Ser473)Akt, anti-GSK3β, anti-phospho-(Ser9)GSK3β, anti-phospho-α subunit of eukaryotic initiation factor 2 (eIF2α), and anti-cleaved caspase 3 (all from Cell Signaling, New England Biolabs, Frankfurt, Germany). Nonimmune rabbit, goat, or mouse IgG was from Sigma-Aldrich Chemie (Buchs, Switzerland). Secondary antispecies antibodies coupled to horseradish peroxidase (HRP) were from Southern Biotechnology (BioReba AG, Reinach, Switzerland), and secondary Cy2- and Cy3-labeled IgG were from Jackson ImmunoResearch Laboratories (West Grove, PA).

Adenovirus- and lentivirus-mediated protein overexpression. Adenovirus-mediated overexpression of human T-cad protein in cultured ECs was performed as described previously (23) using empty and LacZ-expressing vectors as negative controls. T-cad protein with c-*myc* tag was expressed in HUVEC using the adenoviral vector-mediated Adeno-X expression system (Clontech, Palo Alto, CA). cDNA encoding human T-cad without the propeptide was obtained by PCR using mRNA from cultured human aortic smooth muscle cells as a template. The c-*myc* tag was ligated to the N terminus of the full-length coding region of mature T-cad cDNA, and the tagged protein was expressed in HUVEC according to the manufacturer's recommendations, as described elsewhere (23). Briefly, T-cad/c-*myc* cDNA was cloned into pShuttle vector, subcloned into Adeno-X viral DNA, and used for transfection of HEK293 cells with Lipofectamine 2000 reagent. Viral particles were collected from transfected cells after four to five lysis-infection cycles, and the viral titer was determined by endpoint dilution assay. HUVEC were infected with viral particles in normal growth medium at a final concentration of 10 to 100 PFU/cell. The level of T-cad/c-*myc* expression was examined by immunoblotting with anti-c-*myc* and anti-T-cad antibodies.

Adenoviral vector encoding constitutively active Akt (34) was kindly provided by Brian A. Hemmings (Friedrich Miescher Institute Basel, Switzerland) and Zhihong Yang (University of Fribourg, Switzerland).

The enhanced green fluorescent protein (EGFP)-integrin β_3 fusion protein sequence in a pcDNA3 vector (4) was a kind gift from B. Wehrle-Haller (Centre Médical Universitaire, Geneva, Switzerland). The protein sequence was cloned into the pWPXL vector (Tronolab, Lausanne, Switzerland). Subconfluent HEK 293T cells were cotransfected with 20 μg of pWPXL vector, 15 μg of packaging plasmid (pCMV-ΔR8.91), and 5 μg of envelope plasmid (pMD2G-VSVG) by the calcium phosphate precipitation method according to the recommendations of the manufacturer (Tronolab). After 16 h the medium was changed, and recombinant lentivectors were harvested 24 h later. This step was repeated twice, supernatants were pooled together, concentrated on a centrifugal concentrator (molecular mass cutoff, 100 kDa), and the lentiviral titer was determined by infection of HeLa cells with serial dilutions of virus following analysis of EGFP fluorescence by fluorescence-activated cell sorting and by real-time quantitative PCR. For infection of target cells virus was diluted in growth medium in the presence of protamine sulfate (5 μg/ml), incubated for 5 min, and added to the cells, and after incubation (4 h) fresh growth medium was added. After 48 h cells were used for experiments.

Immunoprecipitation. Subconfluent HUVEC in 10-cm dishes were infected with empty adenovector or vector encoding T-cad/c-*myc*. After 48 h cells were washed twice with phosphate-buffered saline (PBS) and then lysed for 2 h at 4°C with 200 μl lysis buffer containing Tris-HCl 50 mM (pH 8.0), 100 mM NaCl, 5 mM $CaCl_2$, 0.2% sodium dodecyl sulfate (SDS), 1% Triton X-114, and complete Mini protease inhibitor cocktail (Roche Diagnostics GmbH, Mannheim, Germany). Lysates were clarified by centrifugation at 12,000 rpm for 10 min at 4°C and used immediately for immunoprecipitation. All subsequent incubations were performed at 4°C with rotation. Preclearing was carried out by incubation of samples with 30 μg nonimmune IgG per sample overnight followed by addition of 10 μl protein G-Sepharose 4 FastFlow beads (Amersham GE Healthcare Bio-Sciences, Munich, Germany), further incubation for 2 h, and removal of the beads by centrifugation at 12,000 rpm for 3 min. Precleared supernatants were incubated with 10 μg of either nonimmune or specific antibody per sample overnight and with protein G-Sepharose beads for 2 h. Immunocomplexes bound to beads were pelleted by centrifugation at 3,000 × *g* for 5 min, washed twice with lysis buffer and once with PBS, eluted in 50 μl of 2× SDS-polyacrylamide gel electrophoresis (PAGE) loading buffer at 80°C for 10 min, and separated by SDS-PAGE. Samples of precipitated proteins were resolved on a gradient of 5 to 19% SDS-PAGE. For initial detection of protein bands gels were either fixed and stained using silver staining reagent (Bio-Rad, Glattbrugg, Switzerland) or analyzed by immunoblotting (see below). To prepare samples for sequencing, pro-

tein bands on gels were visualized with Cypro orange (Bio-Rad), excised, washed with 50% methanol and with 25 mM NH_4HCO_3 solution in acetonitrile, dried in vacuo, and stored at −70°C. Immunoprecipitation was repeated on three separate occasions, and protein bands repeatedly appearing in the precipitates were analyzed by mass spectrometry separately as parallels from independent experiments.

Biotinylation of surface proteins. HUVEC overexpressing T-cad/c-*myc* or infected with empty vector were washed twice with cold PBS, and membrane surface were proteins labeled by incubation of HUVEC with 1.5 mg/ml impermeant LC-sulfo-NHS-(+)-biotin (Molecular BioSciences, Socochim SA, Lausanne, Switzerland) for 30 min at 4°C. Then, cells were washed twice for 20 min with 100 mM ice-cold glycine and twice with ice-cold PBS, lysed with Triton X-114-containing lysis buffer, and used for immunoprecipitations as described above. Immunoprecipitation products were analyzed by Western blotting using a streptavidin-horseradish peroxidase conjugate (Sigma-Aldrich Chemie, Buchs, Switzerland).

Preparation of samples for sequencing: trypsin digestion and extraction of gel slices. Identification of coprecipitated proteins was performed by A. Leitner (Institute of Analytical Chemistry and Food Chemistry, Vienna, Austria). For rehydration and reduction of disulfide bonds, gel slices were covered with 5 mM dithiothreitol in 25 mM NH_4HCO_3 (50 to 120 μl per slice, depending on the number of pieces) and incubated at 60°C in a water bath for 15 min. Then, another 30 to 60 μl of 5 mM dithiothreitol was added. After a total of 30 min the supernatant was removed and 55 mM iodoacetamide in 25 mM NH_4HCO_3 was added (50 to 120 μl). Alkylation of free cysteines was performed for 30 min at room temperature in the dark. After removal of the supernatant, the gel slices were washed twice with 50 mM NH_4HCO_3 and four times with acetonitrile. After the second acetonitrile wash, gel slices were cut into smaller pieces with a scalpel to facilitate dehydration. Shrunken gel pieces were dried to completion in vacuo. For digestion the pieces were rehydrated in 80 to 130 μl trypsin solution (proteomics-grade trypsin; 20 μg/ml in 50 mM NH_4HCO_3) and incubated at 37°C in a water bath. After 30 min a further 20 μl of trypsin solution was added to each sample and digestion was continued overnight at 37°C. Supernatants were transferred to polypropylene tubes and the slices extracted stepwise as follows: (i) acetonitrile-water, 30:70 (vol/vol) containing 1% trifluoroacetic acid (TFA); (ii) 1% TFA in water; (iii) acetonitrile-water, 70:30 (vol/vol) containing 1% TFA. Steps i and ii were performed by shaking for 30 min and sonicating for 3 min. Step iii was performed by shaking for 60 min and sonicating for 3 min. Supernatants from each extraction step were combined, and solvent was removed under nitrogen. Prior to analysis samples were reconstituted in 20 μl acetonitrile-water, 5:95 (vol/vol), containing 0.1% formic acid.

Nano-LC-MS/MS analysis of digests. Nanoflow liquid chromatography-tandem mass spectrometry (nano-LC-MS/MS) was performed on an Agilent Nanoflow Proteomics solution system consisting of an Agilent 1100 series nano-LC system and an Agilent 1100 MSD Trap SL quadrupole ion trap mass spectrometer equipped with an orthogonal nanoelectrospray source; 8-μm inner diameter (ID) nano-ESI tips from New Objective were used. Four-microliter aliquots of the sample solutions were injected onto an Agilent Zorbax 300 SB-C_{18} trapping column (5 mm by 300 μm ID), and the sample was washed for 5 min using 0.05% formic acid in water at a flow rate of 30 μl/min. Then, the trapping column was switched in-line with an Agilent Zorbax 300 SB-C_{18} analytical capillary column (50 mm by 75 μm ID). Gradient elution was performed using the mobile phases A (0.1% formic acid in water) and B (0.1% formic acid in acetonitrile). The gradient was as follows: 0 to 30 min from 5% B to 50% B, 30 to 35 min from 50% B to 80% B, 35 to 40 min 80% B. The flow rate was set to 300 nl/min. MS/MS detection was performed in the data-dependent mode, choosing the two most abundant ions from each full scan in the mass range of 400 to 1,500 *m*/*z*. Dynamic exclusion was used for 2 minutes after the acquisition of two MS/MS spectra. Tandem MS spectra were acquired in the mass range of 300 to 2,000 *m*/*z*. MS/MS spectra were processed using the instrument software, exported as MASCOT (.mgf) files, and searched against either the Swiss-Prot database or the IPI human database using MASCOT 2.0 software. Parameter settings were as follows: taxonomy = homo sapiens (Swiss-Prot only); enzyme = trypsin, up to one missed cleavage, carbamidomethylation on Cys and oxidation on Met as variable modifications; charge states = 1+/2+/3+; instrument = ESI-Trap. Matched proteins were either classified as definite hits or highly likely hits when they fulfilled the following criteria. Definite hits had a significant protein hit according to the MASCOT score in both LC-MS runs; were not classified as a contaminant (keratin); were identified with at least three high-confidence peptide hits; had satisfactory spectral quality with at least four annotated fragment ions; and had reasonable agreement with molecular weight information from gel electrophoresis. Highly likely hits had a significant protein hit according to the MASCOT score in one LC-MS run; were not classified as a contaminant (keratin); were identified with at least one high-confidence peptide hit and other possible hits; had satisfactory spectral quality with at least four annotated fragment ions; and had reasonable agreement with molecular weight information from gel electrophoresis.

Immunofluorescence microscopy. HUVEC were plated at a density of 10^5 cells/well onto 0.5% gelatin-precoated round 12-mm glass coverslips in 24-well plates. For double staining of T-cad and integrin β_3, cell monolayers were scrape wounded to enable analysis of migrating cells. After 18 to 24 h of incubation cells were washed with PBS, fixed with 4% paraformaldehyde, preblocked in PBS containing 0.5% bovine serum albumin (BSA), and incubated with anti-integrin β_3 IgG (1:100) overnight at 4°C and anti-T-cad IgG (1:250) for 2 h at room temperature, followed by staining with secondary anti-species Cy2- and Cy3-labeled IgG diluted 1:500 in blocking solution and applied for 2 h at room temperature. Single staining for intracellular Grp78 was performed on fixed cells after permeabilization with 0.1% Triton X-100. For double staining of surface Grp78 and cadherins, live HUVEC were incubated for 1 h at 37°C with goat anti-Grp78 IgG diluted 1:100 in basal medium containing 3% BSA, rinsed with PBS, and fixed for consecutive staining with anti-T-cad or anti-VE-cadherin (1:200) and secondary Cy2- and Cy3-labeled IgG as described above. For nonspecific controls, nonimmune species IgG replaced the primary antibodies. Coverslips were mounted upside down on slides using FluorSave mounting medium (Calbiochem, Darmstadt, Germany). Single-stained samples were studied under a Zeiss Axiophot fluorescence microscope (Zeiss, Feldbach, Switzerland), and photos were taken using a digital camera and AnalySIS software (Soft Imaging System GmbH, Munich, Germany). Double-stained samples were examined using a laser scanning confocal microscope (LSM 5410; Zeiss, Feldbach, Switzerland). Images were processed and analyzed for colocalization on an O^2 Workstation (Silicon Graphics Computer Systems, Mountain View, CA) using Imaris 3.0 and Colocalization Bitplanes software (Bit Plane AG, Zurich, Switzerland). Nonspecific controls were used to identify a threshold intensity which eliminated >99% of the voxels in these images. Colocalization values were calculated as averages from 20 cell images. Typical micrographs are presented below.

siRNA transfection. Grp78 silencing in HUVEC was performed using previously validated short interfering RNAs (siRNA), 5′-GGAGCGCAUUGAUAC UAGAD-TdT-3′ and 5′-UCUAGUAUCAAUGCGCUCCD-TdT-3′, as annealed oligonucleotides (56). Nonsilencing siRNA proven to have no influence on Grp78 expression at both transcriptional and protein levels (5′-AAGGUGG UUGUUUUGUUCAD-TdT-3′ and 5′-UGAACAAAACAACCACCUUD-Td T-3′) was used as a negative control. siRNA oligonucleotides were purchased from Microsynth (Balgach, Switzerland). Transfection was performed using siPORT reagent (Ambion, Cambridgeshire, United Kingdom) according to the manufacturer's recommendations, and cells were analyzed 72 h posttransfection. The efficiency of silencing, routinely determined by immunoblotting, ranged between 70 and 80%.

Immunoblotting. The method of immunoblotting has been described previously (31). The following primary antibodies were used: anti-T-cad at 1:1,000; anti-c-*myc* at 1:500, mouse anti-Grp78 at 1:1,000, anti-integrin β_3 at 1:500, anti-Akt and anti-phospho-(Ser^{473})Akt at 1:1,000, anti-GSK3β and anti-phospho-(Ser9)GSK3β at 1:1,000, anti-cleaved caspase-3 at 1:500, and anti-GAPDH at 1:3,000. The Amersham enhanced chemiluminescence system (Pierce, Rockford, IL) or Pierce SuperSignal West Dura were variously used for detection of immunoreactive proteins. Scanned images of immunoblots were analyzed using Scion Image (NIH) software. Figures show representative immunoblots.

Cell survival and apoptosis assays. To measure cell survival rates and apoptosis under stress conditions, HUVEC were plated onto 96-well plates or 6-well plates, respectively, at a density of 3×10^4 cells/cm^2, cultured in normal growth medium for 18 h, subjected to a 6-h period of serum deprivation (incubated in Dulbecco's modified Eagle's medium supplemented with 0.1% BSA), and then rinsed with PBS. Survival was measured by cell enumeration using a Coulter Counter or crystal violet staining. For apoptosis assay cells were lysed and immunoblotted with anti-cleaved caspase-3 antibodies. The validity of cleaved caspase-3 immunoblotting for apoptosis detection was tested by comparing immunoblotting data with data obtained from concomitant flow cytometric analysis of annexin V binding. Staining of cells with annexin V-fluorescein isothiocyanate was performed using an ApoAlert kit (Clontech, Palo Alto, CA) according to the manufacturer's standard protocol and analyzed using a DakoCytomation cyan flow cytometer and Summit software (DakoCytomation, Fort Collins, CO). A fluorescence-based Sytox green inclusion assay of cell death (Invitrogen, Molecular Probes, LuBioScience GmbH, Luzern, Switzerland) was performed according to the manufacturer's recommendations using a fluorescence enzyme-linked immunosorbent assay reader. In some experiments anti-Grp78 IgG or nonimmune IgG (at 10 μg/ml) was added to normal growth medium 30 min before

serum deprivation and also included during the full 6-h period of serum deprivation.

Real-time PCR. HUVEC were seeded in six-well plates and transfected with control or Grp78 siRNA. Isolation of RNA, reverse transcription, and real-time PCR analysis were performed as described previously (27). The expression of target molecules was normalized to the expression of β_2-microglobulin. Primer sequences are available on request.

Isolation of rafts. Lipid rafts were isolated on the basis of their insolubility in Triton X-100 and their low buoyant density in sucrose gradients as described previously (42).

Statistical analysis. Unless otherwise stated all results are given as means ± standard deviations (SD). All experiments were performed on at least three separate occasions. Statistical analyses were performed by one-way analysis of variance followed by post hoc Bonferroni's multiple comparison when appropriate using Prism 3.0 software. A P value of <0.05 was considered significant.

RESULTS

Overexpression of tagged T-cad/c-*myc* protein in HUVEC. The first experimental objective of this study was to identify putative membrane partners for T-cad by coimmunoprecipitation. Our previous experiments demonstrated that polyclonal antibodies against human recombinant T-cad produced in our lab are efficient on Western blotting and immunocytochemistry, but not for immunoprecipitation. A number of commercially available anti-T-cad antibodies were tested and also found unsuitable for immunoprecipitation. Therefore, we generated adenoviral vector encoding T-cad protein with c-*myc* tag in order to be able to use commercially available anti-c-*myc* tag antibodies for pull-down of T-cad. Overexpression of c-*myc*-tagged mature T-cad protein was confirmed by Western blotting with anti-c-*myc* and anti-T-cad antibodies (Fig. 1A); blots demonstrate the presence of a major 105-kDa band corresponding to the mature form of T-cad without propeptide and also a minor 90-kDa band which is often observed in cells endogenously expressing T-cad and might be a result of alternative posttranslational modification, i.e., glycosylation.

Immunoprecipitation of tagged T-cad/c-*myc* protein and identification of coprecipitated proteins. Coprecipitation is widely used for studying protein-protein interactions. However, this method is prone to artifacts since its results critically depend on the solubilization conditions. This is particularly relevant in the case of proteins which, like T-cad, are localized within caveolae or lipid raft membrane domains. These membrane compartments are resistant to lysis by many detergents, and insufficient solubilization may result in mistaking nonspecific location of molecules in lipid rafts for direct protein interactions. To avoid this we performed coprecipitation after cell lysis in the presence of Triton X-114, a raft-solubilizing detergent that has been successfully used for identification of molecules specifically associating with GPI-anchored proteins (19).

Immunoprecipitation of lysates from HUVEC expressing c-*myc* tagged T-cad with specific anti-c-*myc* antibodies yielded six protein bands that were reproducibly observed in three independent experiments but were absent in control samples, namely, nonimmune antibody precipitates from c-*myc*/T-cad-expressing cells and nonimmune or anti-c-*myc* antibody precipitates from empty vector-expressing cells (Fig. 1B). Other bands that either variably appeared in both control and "specific" precipitates (i.e., anti-c-*myc* IgG precipitates from c-*myc*/T-cad-expressing cells) or that were irreproducibly present in

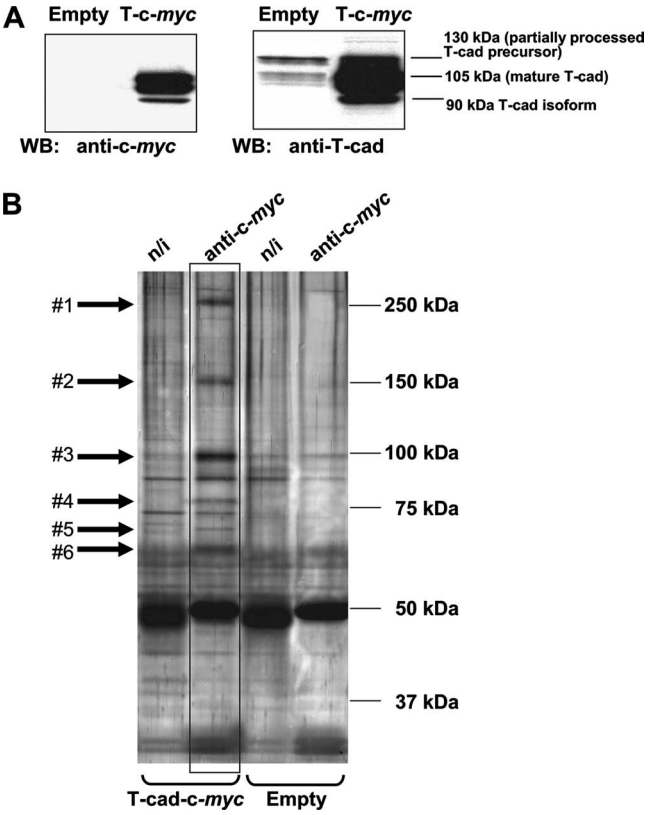

FIG. 1. Precipitation of c-*myc*-tagged T-cad and identification of coprecipitated proteins. (A) Efficiency of adenovirus-mediated overexpression of c-*myc*-tagged T-cad in HUVEC was confirmed by Western blotting with anti-c-*myc* and anti-T-cad antibodies. Empty, control empty vector-infected cells; T-c-*myc*, cells expressing c-*myc*-tagged T-cad. (B) Immunoprecipitation from T-cad/c-*myc*-infected and empty vector-infected cells was performed using anti-c-*myc* antibodies or nonimmune rabbit IgG. Samples were subjected to electrophoresis in SDS-polyacrylamide gels, and protein bands were detected by silver staining. Arrows 1 to 5 indicate protein bands specifically coprecipitated with T-cad, i.e., present only in anti-c-*myc* IgG precipitate from T-cad/c-*myc*-expressing cell lysates (the second lane from the left, marked by the frame) and not in control samples (precipitates from c-*myc*/T-cad-expressing cells by nonimmune antibodies or from empty vector-expressing cells by nonimmune or anti-c-*myc* antibodies).

"specific" precipitates (e.g., present in one experiment but not another) were not considered for subsequent mass spectrometry analysis.

To identify the six reproducibly precipitated proteins, the bands were excised from gels and subjected to nanoflow liquid chromatography-mass spectrometry analysis. Table 1 summarizes the sequence coverage of the proteins identified. Of the six bands, the high-molecular-weight protein (Fig. 1B, band 1) was not positively identified. In the other five bands two proteins were unambiguously identified and classified as definite hits, namely T-cad, or cadherin-13 (bands 3, 4, and 5), and 78-kDa glucose-related protein (band 5), and five proteins were considered highly likely hits, namely, collagen alpha 2 (I) chain (band 2), integrin β_3 (band 4), GABA receptor α1 subunit (band 6), and hypothetical proteins LOC124245 and FLJ32070 (bands 2 and 4).

TABLE 1. Nano-LC and mass spectrometry identification of proteins coprecipitated with T-cad

Protein band no.[a]	Mol mass (kDa)	Match in database
1	~200–250	Not identified
2	~140–150	Hypothetical protein LOC124245 or FLJ32070, collagen alpha 2 (I) chain
3	~100	T-cadherin
4	~75	T-cadherin, integrin β_3, hypothetical protein LOC124245 or FLJ32070
5	~70	T-cadherin, glucose-related protein Grp78/BiP
6	~60	GABA-A receptor α-1 subunit

[a] See Fig. 1B for further illustration.

T-cad associates with Grp78 and integrin β_3 in HUVEC: confirmation of mass spectrometry results by immunoprecipitation and Western blotting. Of the polypeptides coprecipitated with T-cad the most interesting in terms of their possible role in T-cad-elicited signal transduction were Grp78/BiP, a molecular chaperone playing an important role in the unfolded protein response (UPR) that is a survival mechanism initiated by endoplasmic reticulum (ER) disturbances (33), and integrin β_3, which has been shown to participate in EC migration, growth, and survival (47). The next series of experiments aimed to corroborate the T-cad association with Grp78 and integrin β_3. In order to exclude any artifacts due to immunoprecipitation conditions or T-cad overexpression, we repeated immunoprecipitation using two different approaches. First, anti-c-*myc* antibody precipitates from T-cad/c-*myc*-overexpressing HUVEC were subjected to Western blotting analysis with anti-Grp78 and anti-integrin β_3 IgG. Figure 2A confirms the presence of both proteins in the precipitates. No immunoreactivity for T-cad, Grp78, or integrin β3 could be detected by Western blot analysis of anti-c-*myc* antibody precipitates from untransfected cells (data not shown), further confirming the specificity of c-*myc* antibody immunoprecipitates from T-cad/c-*myc*-overexpressing HUVEC. Second, reciprocal immunoprecipitation with anti-Grp78 and anti-integrin β_3 antibodies was performed on parental HUVEC, and immunoprecipitates were analyzed for the presence of T-cad. In the case of integrin β_3, mouse anti-integrin β_3 IgG from BD Biosciences used for Western blotting was not efficient for immunoprecipitation of integrin from cell lysates (not shown). However, the antibody against integrin $\alpha_V\beta_3$ (monoclonal antibody 1976Z) effectively precipitated not only integrin but also T-cad (Fig. 2B), demonstrating that it is an $\alpha_V\beta_3$ heterodimer that associates with

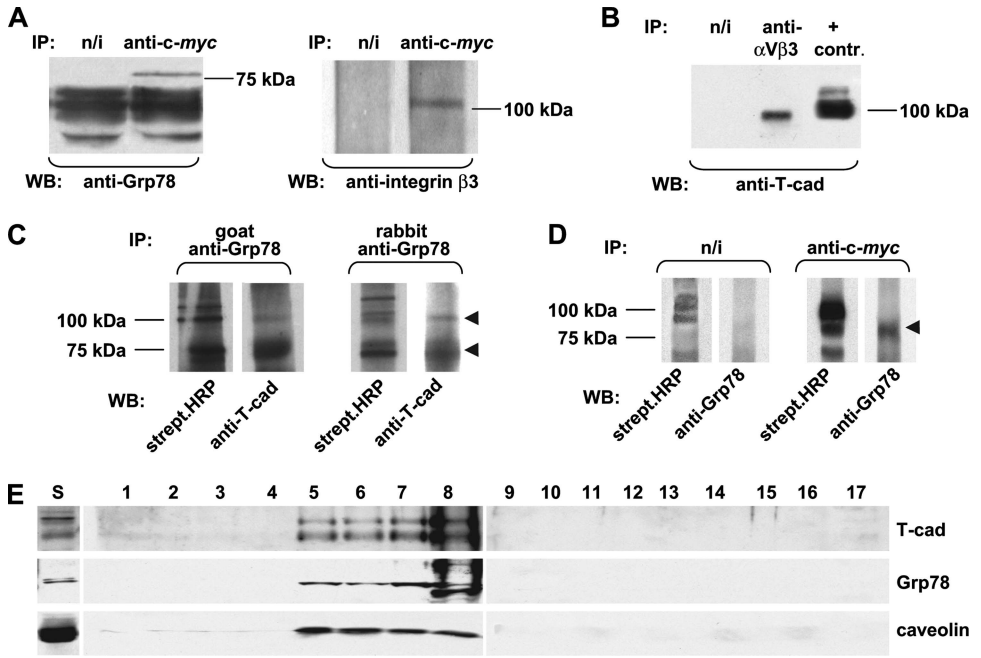

FIG. 2. Confirmation of identity of proteins that coprecipitated with T-cad. (A) Grp78 and integrin β_3 in anti-c-*myc* antibody and nonimmune IgG (n/i) immunoprecipitates (IP) from T-cad/c-*myc*-expressing HUVEC were analyzed by Western blotting (WB) using anti-Grp78 (left panel) or anti-integrin β_3 (right panel) antibodies. (B) The anti-integrin $\alpha_V\beta_3$ antibody IPs from parental HUVEC were analyzed by WB with anti-T-cad antibodies. The positive control for T-cad is HUVEC lysate. (C) To confirm that Grp78 associates with T-cad on the cell surface, precipitation of Grp78 was performed after treatment of parental HUVEC with biotin to label surface proteins. Goat (left panel) or rabbit (right panel) anti-Grp78 antibody immunoprecipitates were analyzed by WB using anti-T-cad antibodies and streptavidin-labeled peroxidase (strept.HRP) to visualize biotinylated proteins. Arrows indicate the protein bands corresponding to T-cad. (D) To confirm that Grp78 associates with T-cad on the cell surface, immunoprecipitation of c-*myc*-tagged T-cad was performed after treatment of T-cad/c-*myc*-expressing HUVEC with biotin to label surface proteins. Anti-c-*myc* antibody (right panel) or n/i IgG (left panel) precipitates were analyzed by WB using anti-Grp78 antibodies (anti-Grp78) and streptavidin-labeled peroxidase (strept.HRP) to visualize biotinylated proteins. The arrow indicates the protein band corresponding to Grp78. (E) Lipid rafts were isolated by density gradient ultracentrifugation of Triton X-100 cell lysates. Fractions (1 to 17 from the top to the bottom of the gradient) were electrophoresed (15 μg of protein per lane) and analyzed by WB for the presence of T-cad, Grp78, and caveolin. S, starting cell lysate.

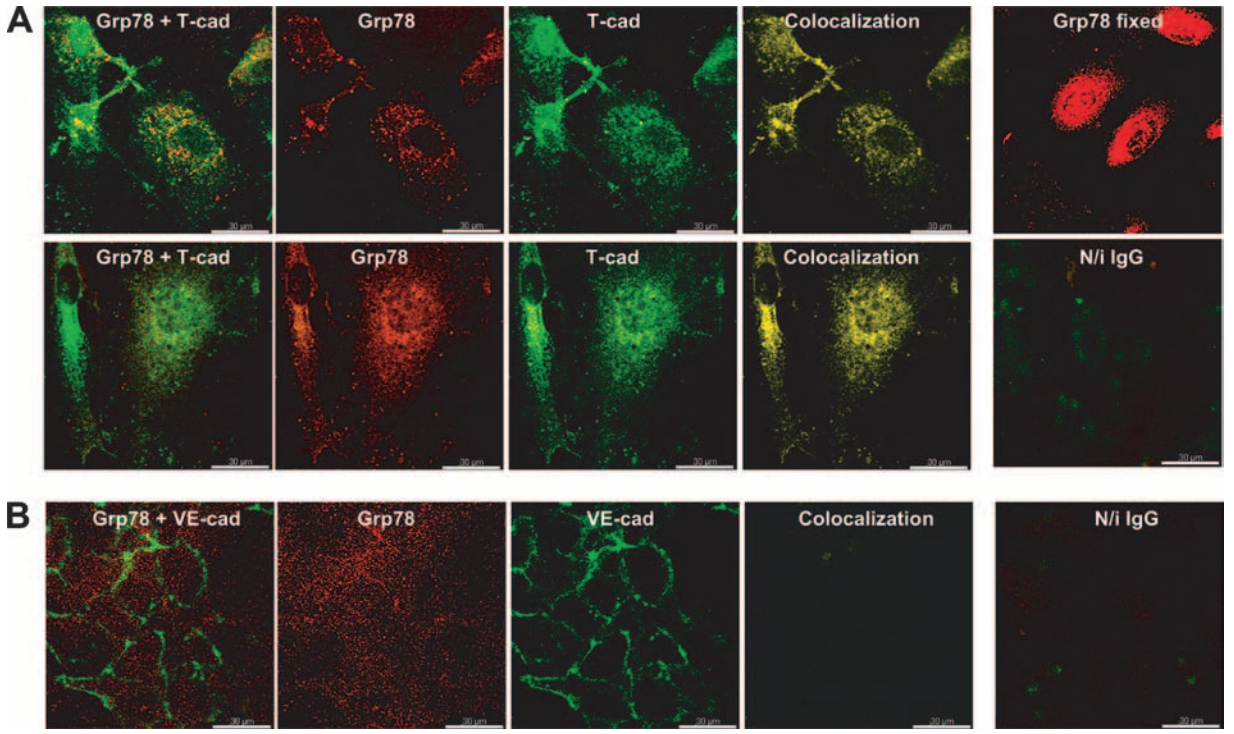

FIG. 3. Confocal microscopy analysis of T-cad colocalization with Grp78 in HUVEC. (A) Double immunostaining for surface Grp78 on live cells and T-cad. Panels labeled Grp78 (red channel) and T-cad (green channel) showed signals from single fluorochrome channels; the panels labeled "Grp78 + T-cad" show merged signals for the two antigens. Confocal analysis to determine precise colocalization of the pixels from individual channels was performed using Imaris 3.0 and Colocalization Bitplanes software and is shown in the colocalization channel (yellow). The negative control (N/i IgG) was double stained with nonimmune (n/i) goat and rabbit IgG (merged micrograph presented). Representative images of two different fields are shown. The image labeled Grp78 fixed (top right panel) shows the Grp78 expression pattern obtained by single staining of fixed and permeabilized cells with anti-Grp78 IgG. (B) Double immunostaining for surface Grp78 on live cells (red channel) and VE-cadherin (green channel). The negative control (far right panel) was double stained with respective n/i control IgG (merged micrograph presented). Colocalization patterns are shown in yellow channel (in both panels A and B). Bar, 30 μm.

T-cad in ECs. Anti-Grp78 antibodies from three different species (mouse, rabbit, and goat) were all able to coprecipitate endogenously expressed T-cad from HUVEC (anti-T-cad immunoblots after either goat or rabbit anti-Grp78 immunoprecipitation are shown in Fig. 2C). Interestingly, anti-Grp78 IgG precipitated not only mature 105-kDa T-cad protein but also a smaller ~75-kDa isoform.

T-cad associates with Grp78 on the surface of HUVEC. Although Grp78 has long been recognized as an intracellular protein localized in the ER, recent data suggest that it is also expressed on the cell surface, where it can act as a signaling receptor. In order to examine whether interactions between Grp78 and T-cad occur on the cell surface, immunoprecipitation was performed after labeling of surface proteins with biotin. T-cad coprecipitated with Grp78 from parental cells by anti-Grp78 antibodies (Fig. 2C) was detected by both anti-T-cad IgG and streptavidin-HRP. Grp78 coprecipitated with c-*myc*-tagged T-cad from T-cad/c-*myc*-overexpressing HUVEC by anti-c-*myc* antibody was detected on Western blotting by both specific anti-Grp78 IgG and streptavidin-HRP (Fig. 2D). These data demonstrate that coprecipitated Grp78 and T-cad proteins are labeled with biotin and therefore associated on the EC surface. A series of Western blotting analyses of lipid rafts isolated from parental HUVEC further demonstrated that both T-cad and Grp78 are located within these plasma membrane domains together with raft marker protein caveolin (Fig. 2E, fractions 5 to 8).

T-cad colocalizes with Grp78 and integrin β_3 in HUVEC: confocal microscopy analysis. The next experiments applied confocal microscopy to directly demonstrate surface colocalization of T-cad with Grp78 and integrin β_3. Most previous studies of Grp78 focused on its main intracellular ER-concentrated pool and revealed strong expression in the perinuclear area. We observed a similar expression pattern after single staining for Grp78 on fixed and permeabilized HUVEC (Fig. 3A, Grp78 fixed). Our confocal studies for T-cad and Grp78 aimed to focus on cell surface Grp78 and to exclude the intracellular Grp78 cellular pool from the analysis. To this end immunostaining with anti-Grp78 antibodies was performed on intact live HUVEC, and only then were cells fixed and probed for T-cad. Parental HUVEC not infected with any viruses and exhibiting endogenous levels of T-cad and Grp78 were used. Staining of live HUVEC with anti-Grp78 antibody showed that Grp78 is distributed in a diffuse manner on the cell surface (Fig. 3A). A similar expression pattern of Grp78 on the surface of prostate cancer cells has been recently reported by Whitaker et al. (58). Combined channel analysis of surface Grp78 and T-cad staining patterns (Fig. 3A) clearly shows surface colocalization of these two proteins in HUVEC. Estimated colocalization values were 35 ± 3.6% and 45 ± 4.3% of total voxel

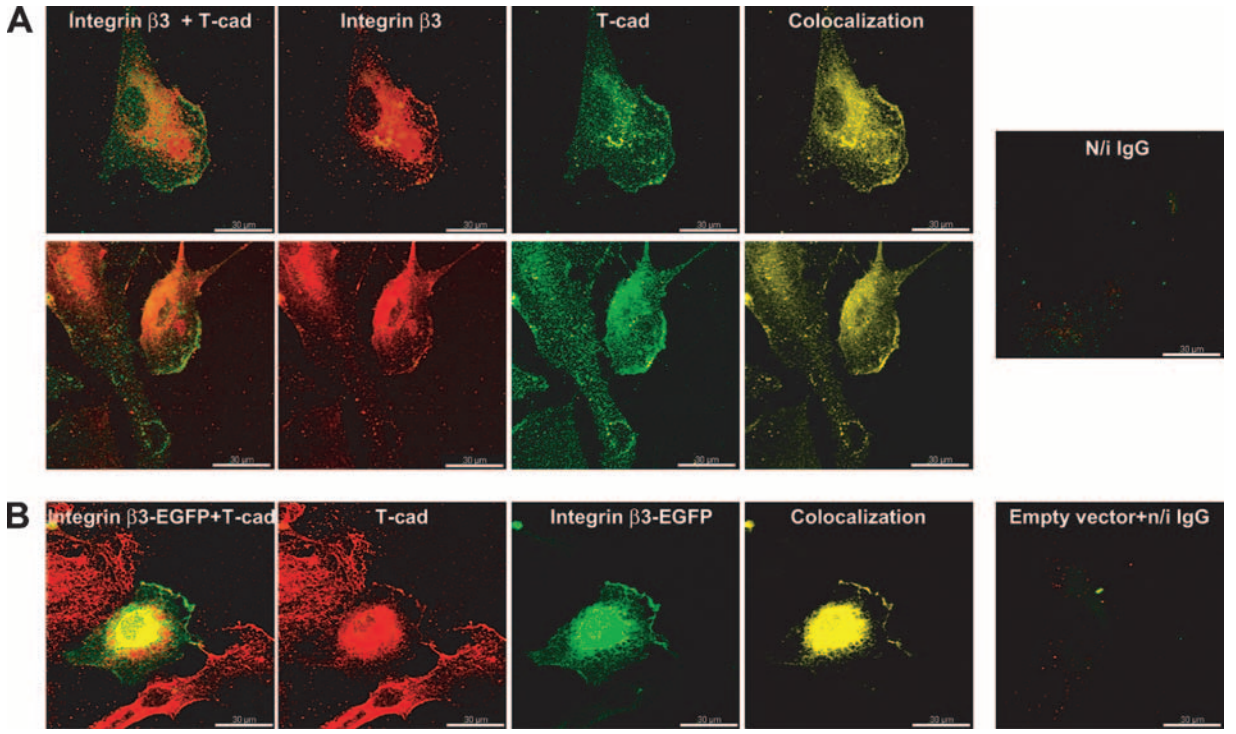

FIG. 4. Confocal microscopy analysis of T-cad colocalization with integrin β_3 in HUVEC. (A) Double immunostaining for integrin β_3 (red) and T-cad (green). The visual combination of signals from red and green channels is shown in the panel labeled "integrin β_3 + T-cad." The colocalization panel (yellow) shows precise colocalization of pixels from separate channels. The negative control (far right panel) was double stained with n/i mouse and rabbit IgG (merged micrograph presented). (B) Immunostaining for T-cad (red channel) in HUVEC expressing the EGFP-integrin β_3 fusion protein (green channel). The negative control is stained empty vector-expressing cells with nonimmune rabbit IgG (far right panel; merged micrograph presented). Colocalization patterns are shown in the yellow channel (A and B). Note the prominent colocalization of integrin β_3 and T-cad at the leading edges of migrating cells (A and B). Bar, 30 μm.

number for Grp78 and T-cad, respectively. Staining for another endothelial cell surface marker, VE-cadherin, performed as negative control, revealed no colocalization with surface Grp78 (Fig. 3B).

Confocal studies for T-cad and integrin β_3 were performed using two different approaches. First, parental HUVEC were double stained for integrin β_3 and T-cad with specific antibodies (Fig. 4A). Secondly, HUVEC expressing integrin β_3-EGFP chimeric protein were stained for T-cad (Fig. 4B). Both approaches revealed colocalization of integrin β_3 and T-cad, with a particularly prominent colocalization pattern at the leading edge of polarized and elongated migratory cells.

Silencing of Grp78 with siRNA attenuates T-cad-induced signaling. We have previously demonstrated that overexpression and ligation of T-cad on ECs activates PI3-kinase/Akt axis signaling and causes related changes in functional responses, such as a decrease in cleaved caspase-3 levels and increased cell survival under conditions of oxidative stress (26). In order to analyze the functional role for Grp78 in T-cad-induced signaling, we first exploited siRNA. The Grp78-specific siRNA used in this study (56) resulted in at least 80% inhibition of Grp78 protein expression 72 h posttransfection (Fig. 5A). Functional efficiency of Grp78 siRNA is proven by the observation that Grp78 knockdown results in further promotion of the ER stress response in cells treated with thapsigargin as judged by stimulation of translation initiation factor eIF2α phosphorylation (Fig. 5A). In control untreated cells and in cells subjected to serum deprivation, Grp78 siRNA also increased phospho-eIF2α levels, although less prominently than in thapsigargin-treated HUVEC (Fig. 5A). Stimulation of ER stress by Grp78 silencing was also demonstrated by upregulation of other genes involved in UPR signaling, namely, TRB3 and vascular endothelial growth factor (see Fig. S1 in the supplemental material), a phenomenon most probably due to the same mechanism that initiates UPR upon a decrease of the free Grp78 ER pool after its sequestration by accumulated misfolded proteins.

Survival-related signaling activation in Grp78 siRNA-transfected cells was measured by Western blotting. We examined immunoblotting for cleaved caspase-3 as a sensitive and reliable readout for apoptosis by comparing immunoblotting data with those obtained from concomitant flow cytometric analysis of annexin V binding, which is a widely accepted quantitative method of early apoptosis detection. The two methods gave concordant results (see Fig. S2 in the supplemental material), thus validating the use of immunoblotting for cleaved caspase-3 to detect apoptosis.

Grp78 siRNA did not exhibit a major influence on the phospho-Akt/caspase-3 axis in control parental HUVEC (Fig. 5B) and in empty vector-transduced HUVEC (Fig. 5C and D) under serum-free conditions. Although there was a tendency toward decreased phospho-Akt and increased cleaved caspase-3 levels in Grp78-silenced cells, analysis of data from multiple experiments showed no statistically relevant difference (Fig.

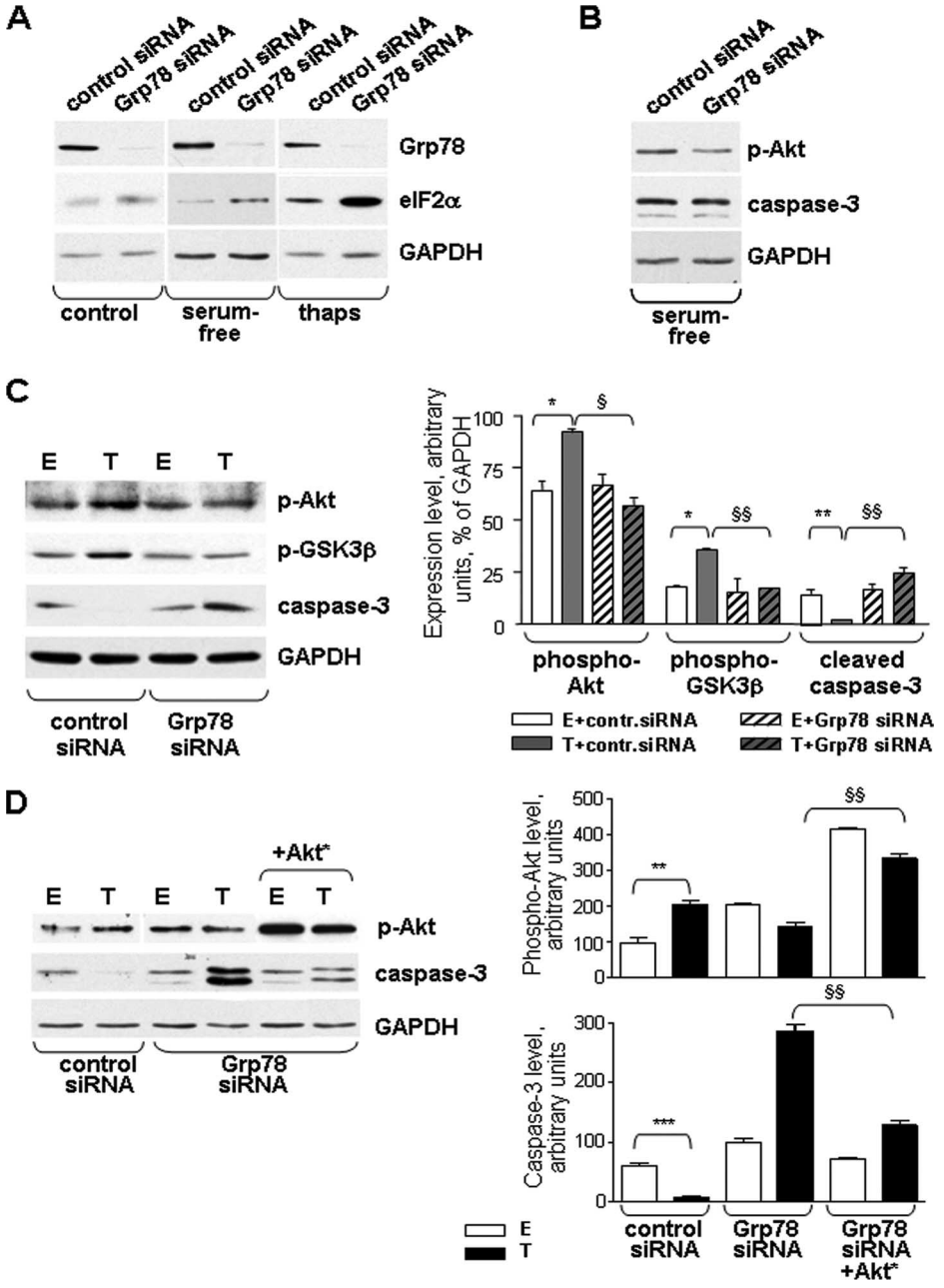

FIG. 5. Silencing of Grp78 with siRNA attenuates activation of Akt/GSK3β signaling pathway in T-cad-overexpressing cells. (A) Efficiency of Grp78 siRNA and its influence on levels of eIF2α in parental HUVEC under normal growing conditions, after 6-h serum deprivation, or after 6-h treatment with 1 μM thapsigargin (thaps) was analyzed by Western blotting. GAPDH was used as an internal control for protein loading. (B) Western blot analysis of the effect of Grp78 siRNA on phospho-Akt and cleaved caspase-3 levels after 6 h of serum deprivation. GAPDH was used as an internal control for protein loading. (C) HUVEC expressing empty adenoviral vector (E) or T-cad (T) were cotransduced with Grp78 siRNA or control siRNA and subjected to serum deprivation for 6 h. Levels of phospho-Akt, phospho-GSK3β, and cleaved caspase-3 were determined by Western blotting and are expressed relative to that of the internal protein loading control GAPDH (arbitrarily taken as 100%). Asterisks indicate significant differences (*, $P < 0.05$; **, $P < 0.01$, between T-HUVEC and the controls E-HUVEC) and § indicates a significant difference (§, $P < 0.05$; §§, $P < 0.01$) between T-HUVEC cotransduced with control or Grp78 siRNA. (D) HUVEC expressing empty adenoviral vector (E) or T-cad (T) were cotransduced with constitutively active Akt mutant, and levels of phospho-Akt and caspase-3 after 6 h of serum deprivation were measured by Western blotting and expressed relative to that of GAPDH. Significant differences: **, $P < 0.01$; ***, $P < 0.001$ (between HUVEC expressing empty adenoviral vector or T-cad). §§, $P < 0.01$ between T-HUVEC cotransduced with control or Akt vectors. Histograms in panels C and D present data (means ± SD) obtained from three independent experiments; representative blots are shown.

5C, graph). Inconsistencies in effects of Grp78 siRNA on phospho-Akt/caspase-3 axis signaling in control cells might be due to subtle differences in the cell preactivation state before the experiment. Taken together, these data suggest that Grp78 per se, although playing an important role in cell survival during ER stress, does not significantly affect prosurvival signaling under the experimental serum-free conditions used in this study.

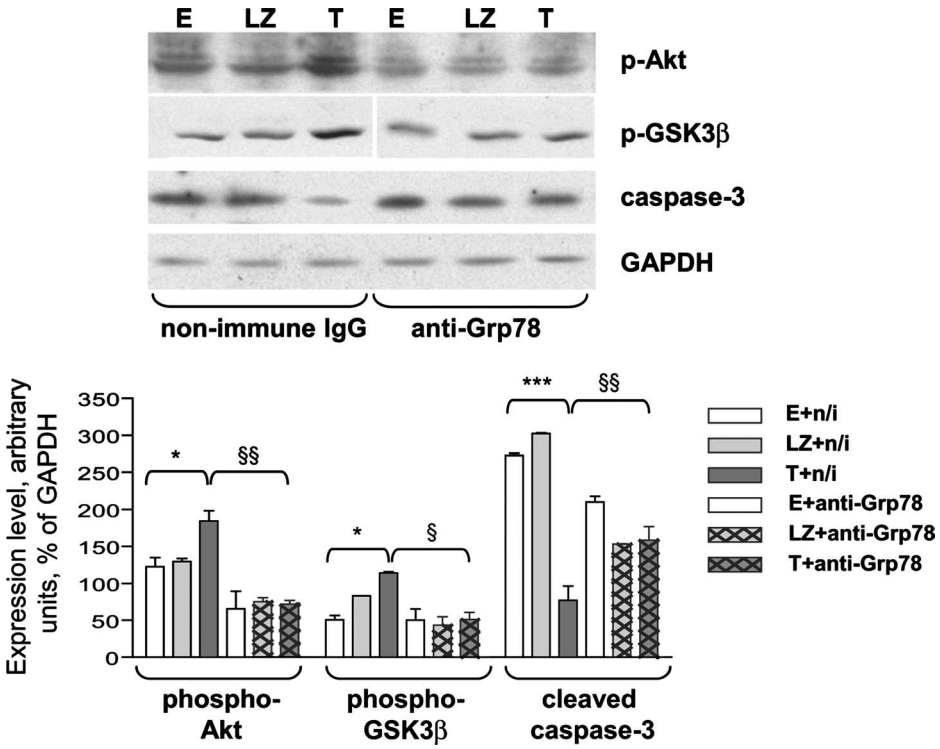

FIG. 6. Function-blocking anti-Grp78 antibodies attenuate activation of the Akt/GSK3β signaling pathway in T-cad-overexpressing cells. HUVEC expressing empty adenoviral vector (E), LacZ (LZ), or T-cad (T) were serum deprived for 6 h with inclusion of either function-blocking anti-Grp78 antibodies or control nonimmune (n/i) IgG (10 μg/ml). Levels of phospho-Akt, phospho-GSK3β, and cleaved caspase-3 were determined in cell lysates by Western blotting; alterations in their levels are expressed relative to that of the internal protein loading control, GAPDH (arbitrarily taken as 100%). Histograms present the data (means ± SD) obtained from three independent experiments, and blots from a single given experiment are shown. Asterisks indicate significant differences (*, $P < 0.05$; ***, $P < 0.001$) between T-HUVEC and either of the controls (E- or LZ-HUVEC), and § indicates a significant difference (§, $P < 0.05$; §§, $P < 0.01$) between T-HUVEC treated with anti-Grp78 antibodies or n/i IgG.

To analyze effects of Grp78 silencing on T-cad signaling, HUVEC or HMEC-1 overexpressing T-cad (T-cad$^+$) and control empty vector were transfected with Grp78 or control siRNA, subjected to stress by serum deprivation, and compared with respect to levels of phospho-Akt, phospho-GSK3β, and cleaved caspase-3. Identical results were obtained for the two cell types; Fig. 5C shows only data for HUVEC. As expected (26), phosphorylation of Akt and GSK3β was increased and the level of active caspase-3 was decreased in T-cad$^+$ cells compared to controls after 6 h of incubation in serum-free medium. Transfection with Grp78 siRNA abrogated T-cad-induced changes in phospho-Akt, phospho-GSK3β, and cleaved caspase-3 levels, bringing them to the same status as in control cells (Fig. 5C). These results indicate that Grp78 is necessary for T-cad signaling through the PI3-kinase/Akt axis. The abrogation of T-cad-dependent prosurvival effects by Grp78 siRNA could be reversed by cotransduction of cells with adenoviral vector encoding constitutively active Akt mutant (Fig. 5D), confirming that Akt is a key downstream mediator of Grp78-coupled, T-cad-dependent survival signaling.

Function blocking of anti-Grp78 antibodies attenuates T-cad-induced signaling. The data shown in the previous section do not permit clear differentiation between the impact of surface and ER-concentrated Grp78, since previous studies reported that silencing of Grp78 with siRNA reduces both the main intracellular Grp78 pool and its surface expression level (35). In order to unequivocally establish the role of the surface Grp78 in T-cad signaling, Grp78 was inactivated on live, intact HUVEC using function-blocking antibodies (goat anti-Grp78 IgG [Santa Cruz]), recognizing the N-terminal end of the Grp78 molecule. Specific or nonimmune antibodies were included in the culture medium both 30 min prior to and during serum deprivation. Similarly to Grp78 siRNA, blocking anti-Grp78 antibodies abrogated effects of T-cad on Akt and GSK3β phosphorylation and caspase-3 activity (Fig. 6). These data demonstrate that it is the interaction between T-cad and Grp78 on the surface of the plasma membrane that is important for T-cad signaling.

Silencing of Grp78 with siRNA and blocking antibodies abrogates T-cad effects on cell survival. To confirm the role for Grp78 role in T-cad survival-related signaling and to test whether the interaction between the two proteins is functionally relevant for EC behavior, we analyzed the effects of Grp78 siRNA and antibodies on T-cad-induced endothelial survival responses. Empty vector- and T-cad-infected HUVEC were transfected with either Grp78-siRNA or control siRNA. Survival was determined after a 6-h period of serum deprivation. Neither Grp78 siRNA (Fig. 7A to C) nor function-blocking anti-Grp78 antibodies (Fig. 7D) per se influenced survival rates of control vector-infected ECs. However, in T-cad-over-

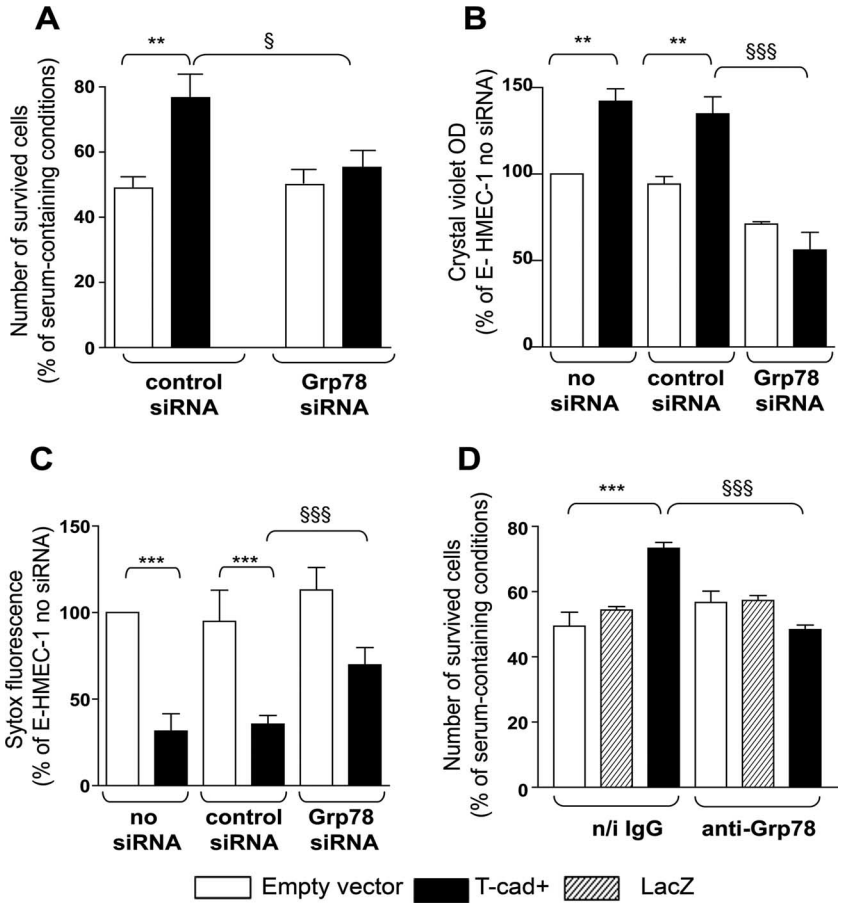

FIG. 7. Silencing of Grp78 inhibits the stimulatory effect of T-cad on cell survival. (A to C) HUVEC expressing empty adenoviral vector (E) or T-cad (T) were cotransduced with Grp78 siRNA or control siRNA and subjected to serum deprivation for 6 h. Differences in cell survival/death rates were determined by enumeration of the surviving cells by using a Coulter Counter (A) or crystal violet staining (B) and by a fluorescence-based assay of Sytox green inclusion (C). (D) E-, LacZ-, and T-cad-infected HUVEC were serum deprived for 6 h with inclusion of either function-blocking anti-Grp78 antibodies or control nonimmune (n/i) IgG (10 μg/ml). The number of surviving cells was determined by cell counting using a Coulter Counter. In panels A to D, survival and death rates after serum deprivation are expressed relative to the respective numbers under control serum-containing conditions (arbitrarily taken as 100%). Histograms present the data (means ± SD) obtained from three independent experiments Asterisks indicate significant differences (**, $P < 0.01$; ***, $P < 0.001$) between T-HUVEC and control E-HUVEC, and § indicates a significant difference (§, $P < 0.05$; §§§, $P < 0.001$) between T-HUVEC cotransduced with control or Grp78 siRNA (A to C) or between T-HUVEC treated with anti-Grp78 antibodies or n/i IgG (B).

expressing HUVEC, which exhibit the expected higher survival rate (26), the prosurvival function of T-cad was abrogated both in HUVEC cotransduced with Grp78 siRNA (Fig. 7A to C) and by inclusion of function-blocking anti-Grp78 antibodies (Fig. 7D).

Silencing of Grp78 with siRNA prevents effects of T-cad ligation. In order to demonstrate that the functional importance of interaction between Grp78 and T-cad is not limited to an artificial system like adenovirus-transduced cells, we tested the effect of Grp78 siRNA on T-cad ligation-dependent signaling in parental HUVEC. An increase in Akt phosphorylation can be induced by homophilic ligation of T-cad on the surface of endothelial cells with our affinity-purified polyclonal rabbit IgG (40) and with goat polyclonal IgG from R&D (Fig. 8A). Grp78 siRNA completely abrogated this ligation-induced stimulation of Akt phosphorylation in normally growing cells (Fig. 8B).

DISCUSSION

This study is the first to report on interactions of GPI-anchored T-cad with other proteins on the cell surface and their possible roles in the transmembrane transduction of signals initiated by surface T-cad engagement.

To search for, and identify, molecular partners for T-cad, we utilized a direct coprecipitation approach with subsequent sequencing of proteins specifically pulled down together with T-cad from lysates of HUVEC expressing c-*myc*-tagged T-cad protein using anti-Tag antibodies. As expected, three definite hits in the precipitate were identified by mass spectrometry as T-cad, confirming the efficiency of immunoprecipitation. Proteins that reproducibly coprecipitated with T-cad included glucose-related protein Grp78/BiP, integrin β_3, collagen α2 (I) chain, GABA-A receptor α1 subunit, and two hypothetical proteins, LOC124245 and FLJ32070. Three of these proteins,

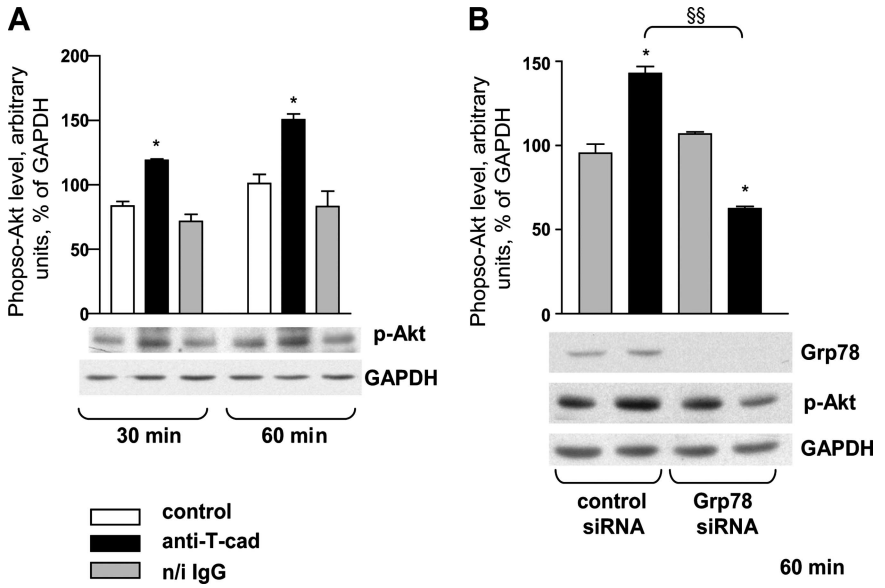

FIG. 8. Silencing of Grp78 inhibits T-cad ligation-dependent activation of the Akt/GSK3β signaling pathway. Parental HUVEC (A) and cells transduced with control or Grp78 siRNA (B) were treated with anti-T-cad antibodies or nonimmune IgG (n/i IgG) diluted in normal growth medium (10 μg/ml) for the indicated intervals. Levels of phospho-Akt, Grp78, and GAPDH were determined in cell lysates by Western blotting. Alterations in phospho-Akt levels are expressed relative to that of the internal protein loading control, GAPDH (arbitrarily taken as 100%). Histograms present the data (means ± SD) obtained from two independent experiments, and representative blots are shown. *, significant difference ($P < 0.05$) between HUVEC treated with anti-T-cad or n/i IgG; §, significant difference ($P < 0.01$) between control or Grp78 siRNA-transduced HUVEC treated with anti-T-cad antibodies.

namely Grp78, integrin β_3, and GABA-A receptor, have been previously shown to localize within lipid rafts (17, 54) (although lipid domains containing GABA-A receptor in rat cerebellar granule cells seem to be a distinct unusual type of rafts, poor in cholesterol and soluble only in the nonionic detergent Brij 98 [11]). It is important to note that even if lipid rafts serve as assembly platforms for T-cad complexes with their partners, interactions between T-cad and the identified proteins were observed even after disruption of lipid rafts with Triton X-114. Therefore, the detected interactions with T-cad are direct and specific and cannot be attributed simply to localization of the proteins within the same membrane compartment. Coprecipitation results were further proven for two of the identified proteins, Grp78 and integrin β_3. These two proteins are involved in the same processes affected by T-cad in ECs (survival, proliferation, and motility) (33, 47) and therefore were considered as the most likely candidates to serve roles as functional adaptors for T-cad. Confirmation of the initial coprecipitation results was done using several independent techniques: detection of Grp78 and integrin β_3 in T-cad precipitates by Western blotting with specific antibodies, reciprocal precipitation using anti-Grp78 and anti-integrin IgGs and detection of T-cad in the precipitates, confocal microscopy, and demonstration of the surface location of the Grp78/T-cad complex by biotinylation of surface proteins prior to precipitation.

Subsequent experiments focused on determining whether Grp78 might be involved in the effects of T-cad on EC survival. Glucose-related protein Grp78 (immunoglobulin heavy chain binding protein, or BiP) belongs to the Hsp70 gene family of stress proteins. The main cellular pool of Grp78 is located in the endoplasmic reticulum, where it works as a molecular chaperone, assisting correct protein folding and assembly and preventing export of misfolded proteins from the ER lumen (16). Grp78 plays an important role in initiating the UPR, the adaptive signaling cascade aimed at protection of cells from conditions causing disturbances in the ER microenvironment, such as accumulation of misfolded proteins, glucose deprivation, disturbances in Ca^{2+} balance and redox regulation, and viral infections, among other things (60). The immediate signaling targets of Grp78 during UPR activation include PERK and Ire1 kinases and transcription factor ATF6, which mediate the initial adaptation response to stress, activation of alarm genes such as NFκB, and finally, if the cell fails to adapt to severe and prolonged ER stress, apoptosis. Many pathophysiological conditions are characterized by cell death induced by ER stress, among them neurodegeneration such as in Alzheimer's and Parkinson's diseases, diabetes, tissue ischemia (hypoglycemia and hypoxia) and reperfusion injury, hyperhomocysteinemia, accumulation of free cholesterol in macrophages, and pathological changes in adipose tissue (reviewed in reference 60). Grp78 has been shown to protect cardiomyocytes from ischemia-induced apoptosis (3, 39, 50, 53) and promote survival of the renal epithelium during oxidative stress. An important role has been attributed to Grp78 in cancer. Grp78 is markedly upregulated in cancer cells, promoting their proliferation, survival, and metastasis and conferring resistance to drugs and T-cell toxicity (reviewed in reference 32). Grp78 may also promote tumor angiogenesis: it mediates glutamine deprivation-induced interleukin-8 and vascular endothelial growth factor proangiogenic signaling in tumor cells (8) and inhibits EC apoptosis caused by topoisomerase inhibitors (9).

Recent data demonstrate that a fraction of the Grp78 cellular pool can escape retention in the ER and translocate to the plasma membrane. There is evidence for low constitutive

surface expression of Grp78 on several cell types, including vascular endothelia (6, 12). Increased levels of surface Grp78 have been detected under pathological conditions on the highly metastatic prostate carcinoma cell line, 1-LN (36), TE671/RD rabdomiosarcoma cells (13), and on endothelial and monocyte/macrophage-like cells in atherosclerotic lesions (6). Grp78 was also present on procoagulant microparticles shed from the plasma membrane of activated ECs (5). When expressed on the cell surface, Grp78 is able to initiate various functional responses: it acts as a coreceptor for dengue virus (24) and coxsackievirus, the latter inducing accumulation of Grp78 and integrin $\alpha_V\beta_3$ within lipid rafts (54), associates with major histocompatibility complex class I molecules (55), complexes with Ro-52 antigen on mouse splenocytes, presumably contributing to autoimmunity during rheumatoid arthritis (44), inhibits procoagulant activity of tissue factor (6), and binds the K5 kringle domain of plasminogen, which results in Grp78 internalization and inhibition of its antiapoptotic effect on procaspase-7 (12).

In the context of the present study, of particular interest are publications by Misra et al., who demonstrated a function for surface Grp78 as a receptor for α2-macroglobulin and delineated its multiple downstream signaling targets. Grp78 mediates α2-macroglobulin-induced intracellular Ca^{2+} elevation and the IP_3 cascade (37) and activates PAK-2, Rac-1, LIMK, and cofilin in a tyrosine kinase- and PI3-kinase-dependent manner that results in increased proliferation and motility (36). α2-Macroglobulin-dependent promotion of proliferation and survival is due to Grp78-mediated activation of PI3-kinase, Akt, ERK 1/2, and p38 mitogen-activated protein kinase, upregulation of Bcl-2, phospho-Bad, phospho-FOXO1, phospho-GSK3β, XIAP, and NF-κB and its upstream activators IKK and IκB, cyclin D1, GADD45, phospho-Ask1, and TRAF2 (35). Our previous work showed that proproliferative and antiapoptotic effects of T-cad are due to initiation of a signaling cascade that includes PI3-kinase, phosphorylation of Akt and GSK3β, activation of β-catenin, and elevation of cyclin D1 (25, 26). Therefore, we considered it plausible that association of Grp78 with T-cad on the cell surface may be functionally relevant and results in activation of pathways common for the two proteins. This hypothesis was tested by examining the effects of both Grp78 transcript silencing and Grp78 function blockade on the ability of T-cad to promote EC survival and to activate related signaling during serum deprivation. T-cad-induced alterations in phospho-Akt, phospho-GSK3β, caspase-3 activity, and survival rates were completely abolished by Grp78 siRNA or blocking antibodies, suggesting that Grp78 indeed functions as a molecular adaptor for lipid-anchored T-cad and that the effects of T-cad on EC survival depend upon formation of a complex with Grp78 on the cell surface.

Establishing the functional relevance of T-cad interaction with other proteins identified by mass spectrometry is beyond the scope of this study. For integrin β_3 we confirmed its colocalization with T-cad by direct and reverse immunoprecipitation and by confocal microscopy. We were able to identify at least one integrin heterodimer containing a β_3 subunit that interacts with T-cad, namely, $\alpha_V\beta_3$. Further circumstantial evidence for T-cad–$\alpha_V\beta_3$ interaction is the presence of the collagen α2 (I) chain in the precipitates. Since denatured collagen type I, a major component of gelatin, is recognized by integrin $\alpha_V\beta_3$ (10), the two proteins might have been pulled down together from HUVEC cultured on gelatin-coated dishes. Our previous data showed that T-cad homophilic ligation and overexpression promotes EC migration and angiogenesis in vitro and in vivo. Interaction with integrins (i.e., $\alpha_v\beta_3$) (47) might be an alternative mechanism which, together with stimulation of proliferation via Akt/GSK3β, contributes to proangiogenic T-cad effects. Accordingly, the most prominent colocalization of T-cad and integrin β_3 was observed at the leading edges of migrating cells, where signaling machinery involved in regulation of motility is concentrated. Integrin-mediated signaling represents a complex network of pathways and effectors, ILK being one of the principal downstream integrin targets (18). We have shown that T-cad-induced activation of Akt and GSK3β depends on ILK (25). It is plausible that T-cad, ILK, integrin β_3, Grp78, and perhaps other signaling molecules form a dynamic multiprotein complex within lipid raft domains of the plasma membrane and differentially contribute to T-cad effects, depending on conditions and cell activation state. Recently, T-cad has been shown to regulate cell-matrix adhesiveness by suppressing integrin β_1 trafficking in cutaneous squamous carcinoma cells (38). One may speculate that differential effects of T-cad in various cell types might depend on its association with different integrins resulting either in promotion or inhibition of cell motility. Interestingly, integrin β_3 coprecipitated with T-cad as two bands of ~100 and ~75 kDa, identified both by mass spectrometry and specific antibodies on Western blots. This might be an artifact related to partial protein degradation during immunoprecipitation and preparation of samples for sequencing. However, as shown for human platelets, where a 60-kDa polypeptide corresponding to the integrin β_{3C} alternative transcript was detected (14), the presence of alternative integrin β_3 isoforms in EC is possible. Ongoing studies in our laboratory are aimed at determining the impact of integrin β_3-T-cad interactions in promigratory and proangiogenic signaling.

Data on the function of GABA receptors, Cl^- channels mediating neurotransmission by gamma-aminobutyric acid, in ECs is limited. GABA-A, -B, and -C receptors are expressed on ECs (61). Chronic GABA-A receptor activation has been shown to influence vascular tone by increasing NO production (28). Interestingly, the present study is not the first to report a connection between GABA receptors and integrins in the endothelium: Shastry et al. demonstrated that GABA-A receptor activation mediates homocystein-induced shedding of integrin β_1 and matrix remodeling by microvascular ECs (48). The deduced sequences of hypothetical proteins LOC124245 and FLJ32070 are based on analysis of genomic DNA; the corresponding polypeptides have not been cloned and described, and their function in the cell is unknown.

Concerning the mass spectrometry results, there was an interesting issue presented by the various protein isoforms identified in the coprecipitates. In vascular EC and smooth muscle cells, T-cad is expressed as two major isoforms, 105 and 130 kDa (mature protein and its partially processed precursor). Additionally, minor ~90-kDa and ~75-kDa bands are occasionally detected in cell lysates (unpublished observations). Takeuchi and colleagues have reported the presence of 80- and 45-kDa T-cad isoforms in human lung extract and in the lung cancer cell line A549 transfected with human T-cad cDNA

sequence obtained from a human brain cDNA library (51). These distinct bands may be the products of alternative splicing, and our preliminary data show that at least some of these forms are polypeptides that diverge in degree of glycosylation. In the current study analysis of c-*myc* coprecipitates revealed the presence of T-cad in three protein bands, namely, in the expected ~100-kDa band 3 (Fig. 1B) and also in the slices excised from the ~75-kDa (band 4) and ~70-kDa (band 5) areas. Possibly some of the endogenously expressed T-cad isoforms might have coprecipitated as a complex with overexpressed c-*myc*-tagged T-cad and T-cad adaptors. Similarly, reverse precipitation of T-cad with anti-Grp78 antibody showed that both 105- and 75-kDa T-cad isoforms coassociate with Grp78, the 75-kDa band being more abundant in the coprecipitates. It could be that the distinct forms of T-cad might interact with diverse sets of molecular partners within the plasma membrane.

The findings in this study are relevant in the context of both the identification of transmembrane signaling partners for GPI-anchored T-cad and the demonstration of a novel mechanism whereby Grp78 can influence endothelial cell survival as a cell surface signaling receptor rather than an intracellular chaperone.

ACKNOWLEDGMENTS

This study was supported by Swiss National Science Foundation grants 3100A0-105406 and 310000-118468/1, EEC grant MOLSTROKE LSHM-CT-2004 contract number 005206, Herzkreislauf Stiftung, and the Swiss Cardiology Foundation.

REFERENCES

1. **Ades, E. W., F. J. Candal, R. A. Swerlick, V. G. George, S. Summers, D. C. Bosse, and T. J. Lawley.** 1992. HMEC-1: establishment of an immortalized human microvascular endothelial cell line. J. Investig. Dermatol. **99:**683–690.
2. **Angst, B. D., C. Marcozzi, and A. I. Magee.** 2001. The cadherin superfamily: diversity in form and function. J. Cell Sci. **114:**629–641.
3. **Azfer, A., J. Niu, L. M. Rogers, F. M. Adamski, and P. E. Kolattukudy.** 2006. Activation of endoplasmic reticulum stress response during the development of ischemic heart disease. Am. J. Physiol. Heart Circ. Physiol. **291:**H1411–H1420.
4. **Ballestrem, C., B. Hinz, B. A. Imhof, and B. Wehrle-Haller.** 2001. Marching at the front and dragging behind: differential αVβ3-integrin turnover regulates focal adhesion behavior. J. Cell Biol. **155:**1319–1332.
5. **Banfi, C., M. Brioschi, R. Wait, S. Begum, E. Gianazza, A. Pirillo, L. Mussoni, and E. Tremoli.** 2005. Proteome of endothelial cell-derived procoagulant microparticles. Proteomics **5:**4443–4455.
6. **Bhattacharjee, G., J. Ahamed, B. Pedersen, A. El-Sheikh, N. Mackman, W. Ruf, C. Liu, and T. S. Edgington.** 2005. Regulation of tissue factor-mediated initiation of the coagulation cascade by cell surface grp78. Arterioscler. Thromb. Vasc. Biol. **25:**1737–1743.
7. **Blasi, F., and P. Carmeliet.** 2002. uPAR: a versatile signalling orchestrator. Nat. Rev. Mol. Cell Biol. **3:**932–943.
8. **Bobrovnikova-Marjon, E. V., P. L. Marjon, O. Barbash, D. L. Vander Jagt, and S. F. Abcouwer.** 2004. Expression of angiogenic factors vascular endothelial growth factor and interleukin-8/CXCL8 is highly responsive to ambient glutamine availability: role of nuclear factor-κB and activating protein-1. Cancer Res. **64:**4858–4869.
9. **Bruneel, A., V. Labas, A. Mailloux, S. Sharma, N. Royer, J. Vinh, P. Pernet, M. Vaubourdolle, and B. Baudin.** 2005. Proteomics of human umbilical vein endothelial cells applied to etoposide-induced apoptosis. Proteomics **5:**3876–3884.
10. **Clark, R. A. F.** 1996. Wound repair: overview and general considerations, p. 3–35. *In* R. A. F. Clark and P. M. Henson (ed.), The molecular and cellular biology of wound repair. Plenum Press, New York, NY.
11. **Dalskov, S. M., L. Immerdal, L. L. Niels-Christiansen, G. H. Hansen, A. Schousboe, and E. M. Danielsen.** 2005. Lipid raft localization of GABA A receptor and Na^+, K^+-ATPase in discrete microdomain clusters in rat cerebellar granule cells. Neurochem. Int. **46:**489–499.
12. **Davidson, D. J., C. Haskell, S. Majest, A. Kherzai, D. A. Egan, K. A. Walter, A. Schneider, E. F. Gubbins, L. Solomon, Z. Chen, R. Lesniewski, and J. Henkin.** 2005. Kringle 5 of human plasminogen induces apoptosis of endothelial and tumor cells through surface-expressed glucose-regulated protein 78. Cancer Res. **65:**4663–4672.
13. **Delpino, A., and M. Castelli.** 2002. The 78 kDa glucose-regulated protein (GRP78/BIP) is expressed on the cell membrane, is released into cell culture medium and is also present in human peripheral circulation. Biosci. Rep. **22:**407–420.
14. **Djaffar, I., Y. P. Chen, C. Creminon, J. Maclouf, A. M. Cieutat, O. Gayet, and J. P. Rosa.** 1994. A new alternative transcript encodes a 60 kDa truncated form of integrin beta 3. Biochem. J. **300:**69–74.
15. **Fredette, B. J., J. Miller, and B. Ranscht.** 1996. Inhibition of motor axon growth by T-cadherin substrata. Development **122:**3163–3171.
16. **Gething, M. J.** 1999. Role and regulation of the ER chaperone BiP. Semin. Cell Dev. Biol. **10:**465–472.
17. **Green, J. M., A. Zhelesnyak, J. Chung, F. P. Lindberg, M. Sarfati, W. A. Frazier, and E. J. Brown.** 1999. Role of cholesterol in formation and function of a signaling complex involving αVβ3, integrin-associated protein (CD47), and heterotrimeric G proteins. J. Cell Biol. **146:**673–682.
18. **Hannigan, G. E., J. G. Coles, and S. Dedhar.** 2007. Integrin-linked kinase at the heart of cardiac contractility, repair, and disease. Circ. Res. **100:**1408–1414.
19. **Hattori, M., M. Osterfield, and J. G. Flanagan.** 2000. Regulated cleavage of a contact-mediated axon repellent. Science **289:**1360–1365.
20. **Horejsi, V., K. Drbal, M. Cebecauer, J. Cerny, T. Brdicka, P. Angelisova, and H. Stockinger.** 1999. GPI-microdomains: a role in signalling via immunoreceptors. Immunol. Today **20:**356–361.
21. **Ivanov, D., M. Philippova, R. Allenspach, P. Erne, and T. Resink.** 2004. T-cadherin upregulation correlates with cell-cycle progression and promotes proliferation of vascular cells. Cardiovasc. Res. **64:**132–143.
22. **Ivanov, D., M. Philippova, J. Antropova, F. Gubaeva, O. Iljinskaya, E. Tararak, V. Bochkov, P. Erne, T. Resink, and V. Tkachuk.** 2001. Expression of cell adhesion molecule T-cadherin in the human vasculature. Histochem. Cell Biol. **115:**231–242.
23. **Ivanov, D., M. Philippova, V. Tkachuk, P. Erne, and T. Resink.** 2004. Cell adhesion molecule T-cadherin regulates vascular cell adhesion, phenotype and motility. Exp. Cell Res. **293:**207–218.
24. **Jindadamrongwech, S., C. Thepparit, and D. R. Smith.** 2004. Identification of GRP 78 (BiP) as a liver cell expressed receptor element for dengue virus serotype 2. Arch. Virol. **149:**915–927.
25. **Joshi, M. B., D. Ivanov, M. Philippova, P. Erne, and T. J. Resink.** 2007. Integrin-linked kinase is an essential mediator for T-cadherin-dependent signaling via Akt and GSK3β in endothelial cells. FASEB J. **21:**3083–3095.
26. **Joshi, M. B., M. Philippova, D. Ivanov, R. Allenspach, P. Erne, and T. J. Resink.** 2005. T-cadherin protects endothelial cells from oxidative stress-induced apoptosis. FASEB J. **19:**1737–1739.
27. **Kadl, A., J. Huber, F. Gruber, V. N. Bochkov, B. R. Binder, and N. Leitinger.** 2002. Analysis of inflammatory gene induction by oxidized phospholipids in vivo by quantitative real-time RT-PCR in comparison with effects of LPS. Vascul. Pharmacol. **38:**219–227.
28. **Kishi, T., Y. Hirooka, K. Sakai, H. Shigematsu, H. Shimokawa, and A. Takeshita.** 2001. Overexpression of eNOS in the RVLM causes hypotension and bradycardia via GABA release. Hypertension **38:**896–901.
29. **Koller, E., and B. Ranscht.** 1996. Differential targeting of T- and N-cadherin in polarized epithelial cells. J. Biol. Chem. **271:**30061–30067.
30. **Kudrjashova, E., P. Bashtrikov, V. Bochkov, Y. Parfyonova, V. Tkachuk, J. Antropova, O. Iljinskaya, E. Tararak, P. Erne, D. Ivanov, M. Philippova, and T. J. Resink.** 2002. Expression of adhesion molecule T-cadherin is increased during neointima formation in experimental restenosis. Histochem. Cell Biol. **118:**281–290.
31. **Kuzmenko, Y. S., F. Kern, V. N. Bochkov, V. A. Tkachuk, and T. J. Resink.** 1998. Density- and proliferation status-dependent expression of T-cadherin, a novel lipoprotein-binding glycoprotein: a function in negative regulation of smooth muscle cell growth? FEBS Lett. **434:**183–187.
32. **Lee, A. S.** 2007. GRP78 induction in cancer: therapeutic and prognostic implications. Cancer Res. **67:**3496–3499.
33. **Li, J., and A. S. Lee.** 2006. Stress induction of GRP78/BiP and its role in cancer. Curr. Mol. Med. **6:**45–54.
34. **Ming, X. F., H. Viswambharan, C. Barandier, J. Ruffieux, K. Kaibuchi, S. Rusconi, and Z. Yang.** 2002. Rho GTPase/Rho kinase negatively regulates endothelial nitric oxide synthase phosphorylation through the inhibition of protein kinase B/Akt in human endothelial cells. Mol. Cell. Biol. **22:**8467–8477.
35. **Misra, U. K., R. Deedwania, and S. V. Pizzo.** 2006. Activation and cross-talk between Akt, NF-κB, and unfolded protein response signaling in 1-LN prostate cancer cells consequent to ligation of cell surface-associated GRP78. J. Biol. Chem. **281:**13694–13707.
36. **Misra, U. K., R. Deedwania, and S. V. Pizzo.** 2005. Binding of activated α2-macroglobulin to its cell surface receptor GRP78 in 1-LN prostate cancer cells regulates PAK-2-dependent activation of LIMK. J. Biol. Chem. **280:**26278–26286.
37. **Misra, U. K., M. Gonzalez-Gronow, G. Gawdi, J. P. Hart, C. E. Johnson, and S. V. Pizzo.** 2002. The role of Grp 78 in alpha 2-macroglobulin-induced signal transduction. Evidence from RNA interference that the low density lipopro-

tein receptor-related protein is associated with, but not necessary for, GRP 78-mediated signal transduction. J. Biol. Chem. **277:**42082–42087.
38. **Mukoyama, Y., A. Utani, S. Matsui, S. Zhou, Y. Miyachi, and N. Matsuyoshi.** 2007. T-cadherin enhances cell-matrix adhesiveness by regulating beta1 integrin trafficking in cutaneous squamous carcinoma cells. Genes Cells **12:** 787–796.
39. **Pan, Y. X., L. Lin, A. J. Ren, X. J. Pan, H. Chen, C. S. Tang, and W. J. Yuan.** 2004. HSP70 and GRP78 induced by endothelin-1 pretreatment enhance tolerance to hypoxia in cultured neonatal rat cardiomyocytes. J. Cardiovasc. Pharmacol. **44:**S117–S120.
40. **Philippova, M., A. Banfi, D. Ivanov, R. Gianni-Barrera, R. Allenspach, P. Erne, and T. Resink.** 2006. Atypical GPI-anchored T-cadherin stimulates angiogenesis in vitro and in vivo. Arterioscler. Thromb. Vasc. Biol. **26:**2222–2230.
41. **Philippova, M., D. Ivanov, R. Allenspach, Y. Takuwa, P. Erne, and T. Resink.** 2005. RhoA and Rac mediate endothelial cell polarization and detachment induced by T-cadherin. FASEB J. **19:**588–590.
42. **Philippova, M., D. Ivanov, V. Tkachuk, P. Erne, and T. J. Resink.** 2003. Polarisation of T-cadherin to the leading edge of migrating vascular cells in vitro: a function in vascular cell motility? Histochem. Cell Biol. **120:**353–360.
43. **Philippova, M. P., V. N. Bochkov, D. V. Stambolsky, V. A. Tkachuk, and T. J. Resink.** 1998. T-cadherin and signal-transducing molecules co-localize in caveolin-rich membrane domains of vascular smooth muscle cells. FEBS Lett. **429:**207–210.
44. **Purcell, A. W., A. Todd, G. Kinoshita, T. A. Lynch, C. L. Keech, M. J. Gething, and T. P. Gordon.** 2003. Association of stress proteins with autoantigens: a possible mechanism for triggering autoimmunity? Clin. Exp. Immunol. **132:**193–200.
45. **Resink, T. J., Y. S. Kuzmenko, F. Kern, D. Stambolsky, V. N. Bochkov, V. A. Tkachuk, P. Erne, and T. Niermann.** 1999. LDL binds to surface-expressed human T-cadherin in transfected HEK293 cells and influences homophilic adhesive interactions. FEBS Lett. **463:**29–34.
46. **Riou, P., R. Saffroy, C. Chenailler, B. Franc, C. Gentile, E. Rubinstein, T. Resink, B. Debuire, D. Piatier-Tonneau, and A. Lemoine.** 2006. Expression of T-cadherin in tumor cells influences invasive potential of human hepatocellular carcinoma. FASEB J. **20:**2291–2301.
47. **Ruegg, C., and A. Mariotti.** 2003. Vascular integrins: pleiotropic adhesion and signaling molecules in vascular homeostasis and angiogenesis. Cell Mol. Life Sci. **60:**1135–1157.
48. **Shastry, S., N. Tyagi, K. S. Moshal, D. Lominadze, M. R. Hayden, and S. C. Tyagi.** 2006. GABA receptors ameliorate Hcy-mediated integrin shedding and constrictive collagen remodeling in microvascular endothelial cells. Cell. Biochem. Biophys. **45:**157–165.
49. **Simons, K., and D. Toomre.** 2000. Lipid rafts and signal transduction. Nat. Rev. Mol. Cell Biol. **1:**31–39.
50. **Szegezdi, E., A. Duffy, M. E. O'Mahoney, S. E. Logue, L. A. Mylotte, T. O'Brien, and A. Samali.** 2006. ER stress contributes to ischemia-induced cardiomyocyte apoptosis. Biochem. Biophys. Res. Commun. **349:**1406–1411.
51. **Takeuchi, T., A. Misaki, J. Fujita, H. Sonobe, and Y. Ohtsuki.** 2001. T-cadherin (CDH13, H-cadherin) expression downregulated surfactant protein D in bronchioloalveolar cells. Virchows Arch. **438:**370–375.
52. **Takeuchi, T., and Y. Ohtsuki.** 2001. Recent progress in T-cadherin (CDH13, H-cadherin) research. Histol. Histopathol. **16:**1287–1293.
53. **Thuerauf, D. J., M. Marcinko, N. Gude, M. Rubio, M. A. Sussman, and C. C. Glembotski.** 2006. Activation of the unfolded protein response in infarcted mouse heart and hypoxic cultured cardiac myocytes. Circ. Res. **99:**275–282.
54. **Triantafilou, K., and M. Triantafilou.** 2003. Lipid raft microdomains: key sites for coxsackievirus A9 infectious cycle. Virology **317:**128–135.
55. **Triantafilou, M., D. Fradelizi, and K. Triantafilou.** 2001. Major histocompatibility class one molecule associates with glucose regulated protein (GRP) 78 on the cell surface. Hum. Immunol. **62:**764–770.
56. **Tsutsumi, S., T. Namba, K. I. Tanaka, Y. Arai, T. Ishihara, M. Aburaya, S. Mima, T. Hoshino, and T. Mizushima.** 2006. Celecoxib upregulates endoplasmic reticulum chaperones that inhibit celecoxib-induced apoptosis in human gastric cells. Oncogene **25:**1018–1029.
57. **Vestal, D. J., and B. Ranscht.** 1992. Glycosyl phosphatidylinositol-anchored T-cadherin mediates calcium-dependent, homophilic cell adhesion. J. Cell Biol. **119:**451–461.
58. **Whitaker, H. C., D. P. Stanbury, C. Brinham, J. Girling, S. Hanrahan, N. Totty, and D. E. Neal.** 2007. Labeling and identification of LNCaP cell surface proteins: a pilot study. Prostate **67:**943–954.
59. **Wyder, L., A. Vitaliti, H. Schneider, L. W. Hebbard, D. R. Moritz, M. Wittmer, M. Ajmo, and R. Klemenz.** 2000. Increased expression of H/T-cadherin in tumor-penetrating blood vessels. Cancer Res. **60:**4682–4688.
60. **Xu, C., B. Bailly-Maitre, and J. C. Reed.** 2005. Endoplasmic reticulum stress: cell life and death decisions. J. Clin. Investig. **115:**2656–2664.
61. **Zhang, Y., and G. Liu.** 1999. A novel method to determine the localization of high and low-affinity GABA transporters to the luminal and antiluminal membranes of brain capillary endothelial cells. Brain Res. Brain Res. Protoc. **4:**288–294.